Integrated Energy Storage Substation Control for Flexible Traction Power System

Yan Li, Fei Lin, Zhongping Yang, Xiaochun Fang, Hu Sun, and Zhihong Zhong

***Abstract*—The deployment of wayside energy storage systems (WESSs) in substations is a key strategy for enhancing the energy efficiency of urban rail transit (URT). Existing research on energy management in traction power system (TPS) with WESS primarily focuses on improving the utilization of surplus regenerative braking energy in the system. However, due to the ambiguous output characteristics of TPS with WESS, it is challenging to address the optimization of overall system energy consumption from the perspective of power flow control, marking a significant distinction from flexible traction power systems (FTPSs) based on bidirectional substations. To address this issue, this paper proposes an integrated energy storage substation (IESS) control method and develops a steady-state equivalent model along with a DC power flow model for TPS with IESSs. Furthermore, under the framework of optimal power flow, this paper achieves both optimized control and flexible power supply for the TPS with IESS. Simulation results based on real-world operation scenarios demonstrate that the proposed method effectively optimizes the TPS power flow and reduces the total system energy consumption, offering new insights into the construction of FTPS based on the IESS.**

***Index Terms*—Urban rail transit, energy storage system, integrated energy storage substation, traction power system, energy management, optimal power flow.**

I. Introduction

With the rapid development of urban rail transit (URT), the power demand of URT is also increasing year by year. According to statistics, by the end of 2024, the total operating mileage of rail transit lines has reached 12160 km in mainland China, with total URT electricity consumption at approximately 27 billion kWh [1]. Traction energy accounts for approximately 50% of the total URT energy consumption, and the regenerative braking energy (RBE) of trains can theoretically reach up to 30%-55% of the traction energy consumption [2]-[4]. The efficient utilization of RBE is one of the key challenges in the field of energy conservation for URT. Energy feedback traction power system (TPS) is a traditional method for recovering RBE, while the bidirectional substation developed from this concept has become a research focus in recent years [5]-[7]. This is because the substations based on bidirectional converter device (BCD) are capable of actively regulating the power output characteristics. This shifts the control focus from passively recovering surplus RBE to actively regulating TPS power flow, thereby reducing the overall system energy consumption including substation losses and line losses. As a result, the optimal power flow (OPF) based approaches have become the standard solution for energy management and control optimization in bidirectional substations. Reference [8] provides a comprehensive review of the achievements of power flow control methods in the energy-saving domain of electrified railways.

Currently, the issues surrounding DC flexible traction power systems (FTPSs) based on bidirectional substations have been extensively discussed [6], [9] - [11]. For distributed TPSs that share the AC grid with the public network, the unidirectional billing policies prevent the feedback energy from delivering direct economic benefits to metro operators, and the poor power quality of feedback can even incur penalties. With advances in storage technologies, the wayside energy storage systems (WESSs) have emerged as an important complementary approach. For the existing lines, installing WESSs on the DC side of substations offers a "plug-and-play" solution with much lower retrofit complexity and cost than AC-side feedback solutions. Additionally, the WESS can serve as an emergency traction power source: when the substation is tripped, the WESS can supply the energy needed to make the affected trains move to the nearest station. A WESS typically consists of energy storage components (such as supercapacitors (SCs), flywheels, or batteries) and a storage converter [12]. Due to the limitations in storage capacity, the available output power of some storage components is coupled with their real-time capacity [13]. For example, the output power of SCs and flywheels is coupled with their real-time capacity and rotational speed, respectively. As a result, the output characteristics of a WESS on the TPS side are inherently coupled with the state of energy storage. In contrast, for AC TPS and BCD-based FTPS, there are no energy capacity constraints, and their output characteristics are fixed, meaning they can always deliver or absorb power based on predetermined behaviors without being affected by such coupling. This fundamental difference must be taken in-

Manuscript received: May 13, 2025; revised: July 13, 2025; accepted: September 11, 2025. Date of CrossCheck: September 11, 2025. Date of online publication: November 25, 2025.

This work was supported by the National Key R&D Program of China (No. 2024YFE0104400).

Y. Li, F. Lin (corresponding author), Z. Yang, X. Fang, H. Sun, and Z. Zhong are with the School of Electrical Engineering, Beijing Jiaotong University, Beijing 100044, China (e-mail: 22110468@bjtu. edu. cn; flin@bjtu. edu. cn; zhpyang@bjtu.edu.cn; hsun1@bjtu.edu.cn; fangxc@bjtu.edu.cn; zhzhong@bjtu.edu.cn).

DOI: 10.35833/MPCE.2025.000412

to account when constructing an FTPS based on WESS.

Due to the aforementioned challenges, most current research on WESS energy management in URT treats WESS merely as an independent and controllable energy storage device. The primary objective is to absorb surplus RBE within the traction power system [14], [15]. Essentially, these studies focus on improving the utilization of existing surplus RBE without considering the active regulation of power flow within the TPS. For instance, the most widely applied strategy in engineering practice is energy management based on traction grid voltage [16] - [19]. The central idea is that the voltage variations in DC traction grid can reflect the energy distribution within the TPS to some extent. In other words, the voltage rises when surplus RBE exists in the system, and drops when there is a residual traction energy demand. Reference [19] sets the charging/discharging voltage thresholds of WESS based on the no-load voltage of the substation and compares them with the grid voltage to determine the WESS operating conditions. However, in distributed TPS, the no-load voltage may vary between substations. Thus, the relationship between no-load voltage and grid voltage alone cannot accurately reflect the energy distribution [20]. Therefore, some researchers have considered controlling WESS directly based on the operating status of trains [20] - [22]. For example, [21] simultaneously monitors the grid voltage, train displacement, and power to infer the distribution of surplus RBE and optimize the WESS control accordingly. Specifically, it integrates the parameters of WESSs with the operation parameters of train into a discrete-time optimization framework, using a unified scheduling model to synchronously determine the charging and discharging actions at each time step. Reference [22] controls the charging/discharging of WESS by tracking the traction and braking power of train motors. In recent years, several studies have also applied various optimization algorithms including machine learning (ML) to address the WESS energy management, particularly for the coordination control of multi-WESSs. For example, [23] integrates the particle swarm optimization (PSO) to optimize the charging/discharging voltage thresholds of different WESSs through voltage-based control rules of traction grid, aiming to reduce the energy consumption of substation and peak power output. Throughout the control and optimization process, the WESS is still treated as isolated controlled object. Reference [24] reviews the application of heuristic optimization algorithms represented by genetic algorithms (GAs) in energy management strategy (EMS) for URT TPS. In the field of ML, particularly with deep reinforcement learning (DRL) as representative algorithm, several studies have explored the applications [25] - [28]. For example, [25] implements a decentralized cooperative control scheme based on multi-agent deep reinforcement learning (DRL) for coordinating multiple WESSs. In this scheme, each WESS functions as an autonomous agent, relying on its local state to make charging/discharging decisions, while a shared global reward mechanism fosters inter-station cooperation, thereby enhancing the recovery efficiency of surplus RBE.

It is evident that the existing studies, which are based on independently controlled model of WESS, essentially focus on determining the operating states of WESS by various optimization methods to maximize the recovery of surplus RBE. Within this framework, the independent control parameters cannot be directly linked to the overall output characteristics of TPS. This represents a passive control approach. In reality, the output behaviors of both substations and WESSs jointly shape the internal energy interactions of the TPS, thereby directly determining system-wide energy distribution. Furthermore, the operating conditions of WESSs can indirectly influence the operating states of substations. Therefore, when designing control strategies, if the substation and WESS are modeled as independent systems from the outset and the previously discussed coupling between power and capacity of energy storage is also neglected, the resulting output characteristics of both the WESS and substation during the actual control and optimization as well as the overall output behavior of TPS remain unclear. In essence, this constitutes a “black-box” process.

To the best of our knowledge, no existing study has yet considered the energy storage and substation as an integrated system in URT TPS. A key question is whether the concept of FTPS, previously realized through bidirectional substation, can be extended to systems based on integrated energy storage substations (IESSs), where WESS actively regulates the output behavior of substation and, in turn, the overall power flow of TPS. Specifically, this would involve controlling power flow to reshape the energy distribution within the system, such that the complete recovery of RBE is achieved while minimizing the total system energy losses. Based on the above, advancing EMS from the perspective of power flow optimization is an important research direction. Given the limitations of current control methods and the inherent coupling characteristics of energy storage, it remains challenging to establish a clear steady-state equivalent model for a TPS with WESS. The ambiguity in the output characteristics further complicates the identification of appropriate control parameters required to achieve the optimal energy efficiency in the TPS. Therefore, it is of significant importance to explore the method of constructing an FTPS based on WESS. Specifically, there are still the following gaps in the focus of this study.

1) The research on the application of WESS still stays in the perspective of simply regarding WESS as an energy storage device. However, the potential of WESS to actively regulate output characteristics of the substation and, consequently, control the overall power flow of the TPS has been overlooked.

2) There is still no control method or EMS that takes WESS and substation as an integrated system. It is necessary to develop a unified model for the output characteristics of IESSs while considering the coupling between the grid side and storage side.

3) The operation mode of energy system based on OPF framework can often achieve the best energy-saving effect. It is important to extend the concept of FTPS implemented via bidirectional substations under the OPF framework to the systems based on IESSs.

To this end, this paper proposes an IESS control method. A case study based on real-world engineering data validates the effectiveness of the proposed method. Simulation results demonstrate that the proposed method allows the TPS power flow to adaptively respond to system-wide traction and braking load demands, thereby realizing the flexible traction power supply. Compared with existing methods, it significantly enhances the overall utilization of RBE and reduces the total energy consumption of TPS. The specific contributions are summarized as follows.

1) This paper proposes integrating the WESS and substation into a unified IESS, which is a new concept, along with the development of a control-oriented modeling framework.

2) The power threshold control is incorporated into the integrated control structure to decouple the grid-side and storage-side interactions. Thus, the controllable output characteristics of IESSs are explicitly described, enabling the system to actively participate in the power flow regulation.

3) A steady-state equivalent model along with DC power flow model of the TPS with IESSs is constructed, which could be embedded into the OPF framework. With the energy-saving as the primary objective, the optimization of IESS control parameters is successfully achieved under the general OPF framework.

The remainder of this paper is structured as follows. Section II analyzes the operating characteristics of TPS in URT. Section III specifically introduces the construction method of the FTPS based on the IESSs. Section IV conducts case studies on the proposed method, and builds a simulation based on real-world engineering data of a metro line in Beijing, China, which verifies the effectiveness of a the proposed method. Finally, Section V summarizes and prospects this paper.

II. Operating Characteristics of TPS in URT

A. Operating Characteristics of Substation

The substation of TPS in URT usually adopts 24-pulse rectifier, which is composed of two 12-pulse traction rectifiers in parallel. In order to simplify the analysis, it is generally approximated as a droop output characteristic with a certain slope [29]. The ideal traction rectifier can be modeled as a voltage source in series with an internal resistance. Its output characteristic is expressed as (1), with a unidirectional conduction characteristic.

$$u_{sub}=u_{s0}-r_{s0}i_{sub}\quad i_{sub}\geq 0 \tag{1}$$

where u_{s0} and r_{s0} are the equivalent voltage and internal resistance of substation, respectively; and u_{sub} and i_{sub} are the output voltage and current of substation, respectively.

The equivalent internal resistance is determined by the characteristics of the traction rectifier itself. The equivalent voltage can be regarded as the no-load voltage of substation, which is determined by the characteristics of traction rectifier and the medium-voltage (10 kV/35 kV) AC grid, expressed as:

$$u_{s0}=\frac{\sqrt{2}\,n}{\pi}\eta u_{ac}\sin\frac{\pi}{n} \tag{2}$$

where n is the rectifier pulse number; η is the turn ratio of traction transformer; and u_{ac} is the voltage of AC grid.

Therefore, for a general substation, when the parameters of the traction rectifier and traction transformer are determined, the output characteristics of the DC side indicate a rigid system, and the output of TPSS is not adjustable.

B. Operating Characteristics of WESS in URT

The WESS in URT connects the energy storage with the DC traction grid by the DC/DC converter, as shown in Fig. 1. The common SC or lithium battery is taken as an example of energy storage components. The DC/DC converters widely use a double-loop control structure with an outer voltage loop and an inner current loop (or variants such as a power loop) [16], as shown in Fig. 2, where PI and PWM are short for proportional-integral and pulse width modulation, respectively. Since the installation of WESS in substations is the most common practice [30], the actual bus voltage of DC/DC converter is generally equal to the substation voltage at the installation location. An obvious advantage of this method is that the operation will be directly controlled by the voltage of DC traction grid.

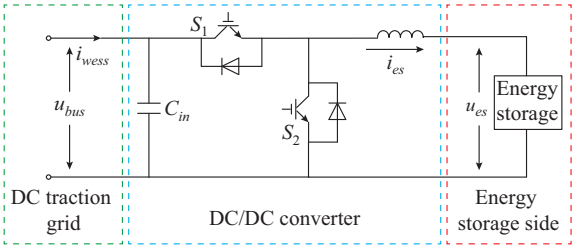

Fig. 1. WESS structure in URT.

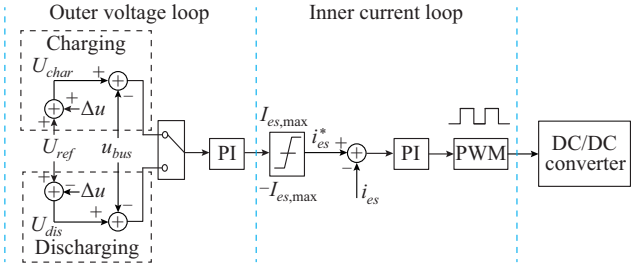

Fig. 2. Double-loop control structure for DC/DC converter.

Limited by the current stress of the power device and the energy storage itself, it is usually necessary to carry out limiting operation of the current output from the outer loop. If the current loop is regarded as ideal, the current on the energy storage side can be obtained as:

$$i_{es}=\begin{cases}k_p(U_{thres}-u_{bus})+k_i\int(U_{thres}-u_{bus})\mathrm{d}t & |i_{es}|<I_{es,\max}\\ \pm I_{es,\max} & |i_{es}|\geq I_{es,\max}\end{cases} \tag{3}$$

where $U_{thres}=U_{ref}\pm\Delta u$ is the charging/discharging voltage threshold (U_{char}/U_{dis}), U_{ref} is the given voltage instruction on the grid side of DC/DC converter, and Δu is the hysteresis voltage; u_{bus} is the actual bus voltage of DC/DC converter; k_p and k_i are the proportional and integral coefficients, respectively; and $I_{es,\max}$ is the maximum current limit of energy storage.

The steady-state output characteristics of WESS on the grid side are usually analyzed based on power conservation principle [31] as:

$$u_{bus}i_{wess}=\begin{cases}i_{es}u_{es}/\eta_{wess} & \text{charging}\\ \eta_{wess}i_{es}u_{es} & \text{discharging}\end{cases} \tag{4}$$

where i_{wess} is the WESS current on grid side; u_{es} is the terminal voltage of energy storage; and η_{wess} is the conversion efficiency of WESS.

When the outer voltage loop is saturated, i. e., when the system is operating at the maximum current, the maximum power that the energy storage can provide is defined as $P_{ava,\max}$. Since the conversion efficiency of WESS is usually more than 90% [18], according to (3) and (4), the WESS power on the grid side P_{wess} can be expressed as:

$$P_{wess}\approx P_{ava,\max}=I_{es,\max}u_{es} \tag{5}$$

Formulas (4) and (5) show that regardless of the operating mode of WESS, its steady-state output characteristics on the grid side are always coupled with the energy storage side. This is particularly true for energy storage components such as SC. Due to their high-power density and charging/discharging characteristics that align well with train load profiles, the SCs are widely used in URT. However, the square of the terminal voltage of an SC has a linear relationship with its state of capacity (SOC), shown as:

$$\begin{cases}u_{sc,\min}<u_{sc}<u_{sc,\max}\\ SOC=u_{sc}^2/u_{sc,\max}^2\end{cases} \tag{6}$$

where $u_{sc,\min}$ and $u_{sc,\max}$ are the minimum and maximum limits for the terminal voltage of SC u_{sc}, respectively. When the terminal voltage exceeds the limits, the SC ceases operation.

In other words, when SC is used as an energy storage component, its maximum available power $P_{ava,\max}$ depends not only on its design capacity but also on the real-time capacity, which differs from reversible substations. Figure 3 illustrates the external output characteristics of WESS on the grid side, where $P_{es,\min}$ and $P_{es,\max}$ are the minimum and maximum designed power of energy storage P_{es}, respectively.

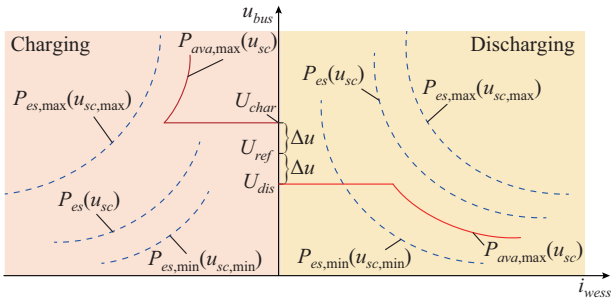

Fig. 3. External output characteristic curve of WESS on grid side.

In Fig. 3, the red solid line indicates the actual operating curve of WESS on the grid side. The blue dashed lines indicate that the power limit of WESS changes with the SOC (or u_{sc}) during operation, which in turn affects its output characteristics on the grid side. This process applies not only to SC but also to flywheel, although the latter uses DC/AC converters and $P_{ava,\max}$ is influenced by the real-time rotational speed. Moreover, even when analyzing the steady-state output characteristics within the constant-voltage region, (4) must still be used as the basis. Therefore, the output characteristic analysis of WESS on the grid side is always coupled with the energy storage side, regardless of the type of storage medium used.

C. Operating Modes of IESS

As discussed earlier, FTPS based on power flow control methods has become an important direction in the development of URT power supply technologies. Figure 4 compares a typical BCD-based FTPS with a conventional rectifier-based TPS. After the BCD parameter design is completed, the output characteristics of the TPS can be determined. Since there is no limit of real-time capacity state, in theory, the output characteristics of substation can be regulated by controlling the BCD. Therefore, the optimal power supply parameters can be designed based on the OPF algorithm according to the train load characteristics and grid topology.

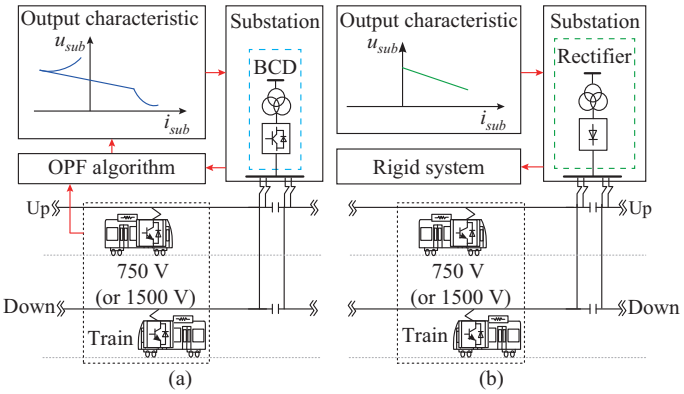

Fig. 4. Schematic diagram of BCD-based FTPS and REC-based TPS. (a) BCD-based FTPS. (b) Rectifier-based TPS.

Based on the configuration of WESS in URT, it is evident that the operating condition of WESS will also indirectly affect the operation of substation. Therefore, we consider the WESS and substation as an integrated control entity and define a substation equipped with WESS as an IESS. Based on the above analysis of the external output characteristics of the substation and WESS, the operating modes of the IESS can be categorized into six distinct cases, as illustrated in Fig. 5.

Modes a and b correspond to the scenarios where the WESS is cut off. In mode a, the substation operates independently; while in mode b, the entire IESS is deactivated. The corresponding output characteristics in modes a and b are described by:

$$i_{iess}=\begin{cases}\dfrac{u_{s0}-u_{sub}}{r_{s0}} & \text{mode a}\\ 0 & \text{mode b}\end{cases} \tag{7}$$

where i_{iess} is the current of IESS.

Modes c and d correspond to the scenarios where the WESS operates at its maximum available power. In mode c, both the substation and WESS work simultaneously; while in mode d, the WESS operates independently. The corre-

sponding output characteristics in modes c and d are described by:

$$i_{iess}=\begin{cases}\dfrac{u_{s0}-u_{iess}}{r_{s0}}+\dfrac{P_{ava,\max}}{u_{iess}} & \text{mode c}\\ \dfrac{P_{ava,\max}}{u_{iess}} & \text{mode d}\end{cases} \tag{8}$$

where u_{iess} is the node voltage of IESS.

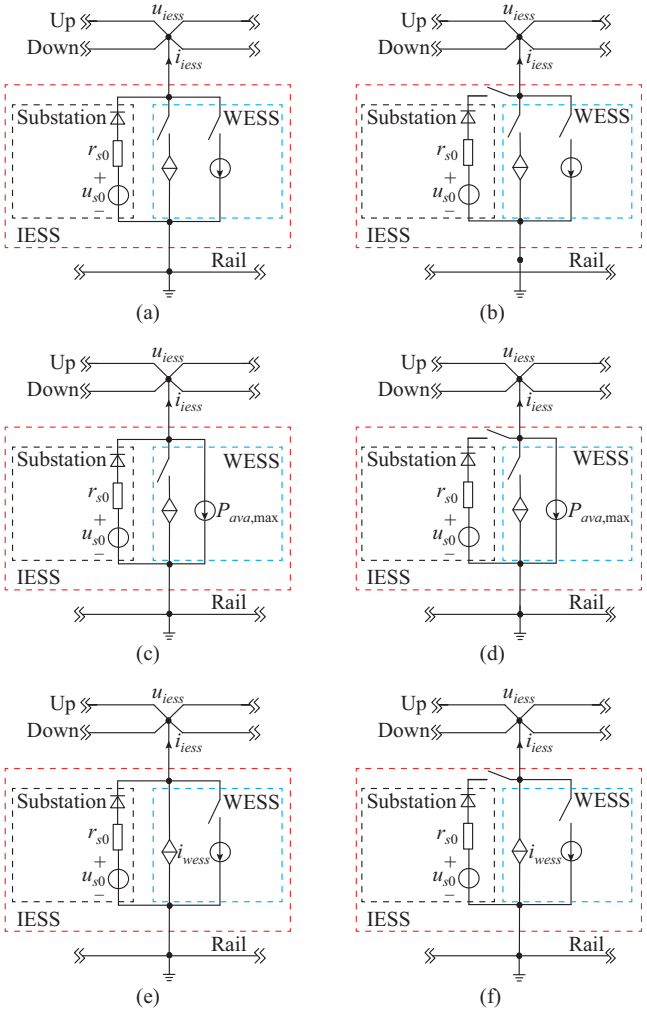

Fig. 5. Operating modes of IESS. (a) Mode a. (b) Mode b. (c) Mode c. (d) Mode d. (e) Mode e. (f) Mode f.

Modes e and f correspond to the scenarios where the WESS does not reach the maximum available power. In this case, WESS can be equivalent to a controlled current source based on the power conservation law according to the above analysis. In mode e, the substation and WESS work simultaneously. In mode f, the WESS works alone. The corresponding output characteristics in modes e and f are described by:

$$i_{iess}=\begin{cases}\dfrac{u_{s0}-u_{iess}}{r_{s0}}+i_{wess} & \text{mode e}\\ i_{wess} & \text{mode f}\end{cases} \tag{9}$$

For modes c-f, combining (4) and (9) as well as (5) and (8), it can be observed that the output characteristics of the IESS remain coupled with the energy storage side, and no unified model has been established, linking the output characteristics with control parameters. As previously discussed, the current methods only determine the WESS state and fail to actively regulate the overall output characteristics of TPS, as is the case with FTPS. Essentially, the current methods fall into the category of passive "black-box" control. The actual output characteristics of the WESS and substation, as well as the overall output characteristics of TPS under these conditions, remain unclear.

III. Construction Method of FTPS Based on IESSs

According to the above analysis, it is necessary to investigate novel control strategies that can render the output characteristics of a TPS with WESS controllable. Moreover, such strategies should be compatible with the general OPF framework to enable active regulation of system power flow, thereby achieving the improved energy-saving performance. Therefore, this paper proposes a construction method of FTPS based on the IESSs.

A. IESS Control Method

Inspired by the widely adopted classical droop control method used in bidirectional substations [32], this paper proposes an IESS control method, as illustrated in Fig. 6. The integrated equivalent control model of IESS is assumed to consists of virtual voltage source and virtual resistor. To achieve the integrated control, the total output current of IESS is used as the input to the droop control, which regulates its output characteristics accordingly. However, since the WESS is the actual device being directly controlled, the output of the droop control is used to adjust the reference value of the outer voltage loop:

$$U_{iess}^{*}=U_{ref}^{*}-r_{ref}^{*}i_{iess} \tag{10}$$

where U_{ref}^{*} and r_{ref}^{*} are the virtual voltage source and resistor, respectively; and U_{iess}^{*} is the reference voltage of IESS.

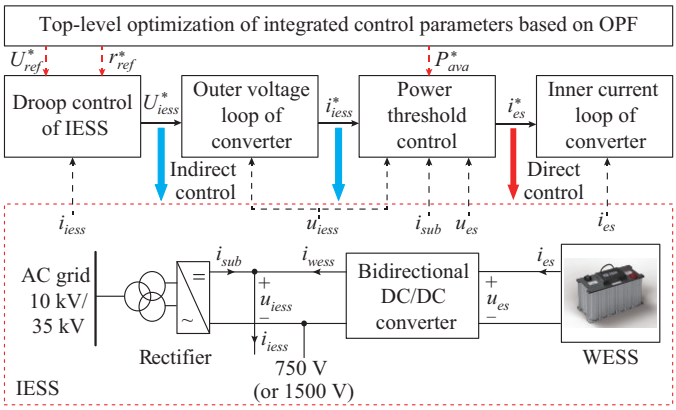

Fig. 6. IESS control method.

The output of the outer voltage loop is used as the overall reference current i_{iess}^{*} for the IESS. On this basis, a power threshold control is introduced to decouple the output characteristics of IESS from those of the energy storage side. First, the WESS current demand on the grid side i_{wess}^{*} is obtained by subtracting the actual current of substation from the IESS

current reference generated by the voltage outer loop. Meanwhile, the power threshold P^*_{ava} is defined as the available power from the energy storage system, which is less than or equal to the maximum deliverable power $P_{ava,\max}$, as determined by (5). Then, based on the principle of power conservation, the final current reference i^*_{es} for the energy storage side is derived. Taking the SC as an example, the control process is expressed as:

$$\begin{cases} i^*_{wess} = i^*_{iess} - i_{sub} \\ P^*_{ava} \le P_{ava,\max} = I_{es,\max} u_{es} \\ i^*_{es} = \max(u_{iess} i^*_{wess}, P^*_{ava})/u_{es} \end{cases} \tag{11}$$

Based on the previously defined operating modes of IESS, when the WESS still has available capacity and remains active, i. e., operating in modes c-f, the output characteristics on the grid side can be described by (12).

$$i_{iess} = \begin{cases} \dfrac{u_{s0} - u_{iess}}{r_{s0}} + \dfrac{P^*_{ava}}{u_{iess}} & \text{mode c} \\ \dfrac{P^*_{ava}}{u_{iess}} & \text{mode d} \\ \dfrac{U^*_{ref} - u_{iess}}{r^*_{ref}} & \text{modes e and f} \end{cases} \tag{12}$$

When the WESS reaches its available power limit, i.e., operating in mode c or d, the IESS is primarily regulated by the power threshold P^*_{ava}. When the WESS operates below its maximum available power, i.e., operating in mode e or f, the IESS is mainly regulated by the droop control parameters U^*_{ref} and r^*_{ref}, and its external output characteristics can be uniformly expressed.

Figure 7 illustrates the external output characteristics of the IESS under the proposed method. Due to the unidirectional conduction characteristic of traction rectifier units, the IESS operates in the energy-storage mode, i. e., the only mode when its output voltage exceeds the no-load voltage of the substation. Under the steady-state analysis, at the intersection of modes d and f, the output power of IESS equals P^*_{ava}. When the output voltage of IESS is lower than the no-load voltage of substation, the intersection of modes c and e in the steady-state analysis satisfies (13). When the WESS is completely depleted and disconnected, the IESS exhibits the same external output characteristics as a conventional substation, operating in mode a or b.

$$u_{iess}\left(\frac{U^*_{ref} - u_{iess}}{r^*_{ref}} - \frac{u_{s0} - u_{iess}}{r_{s0}}\right) = P^*_{ava} \tag{13}$$

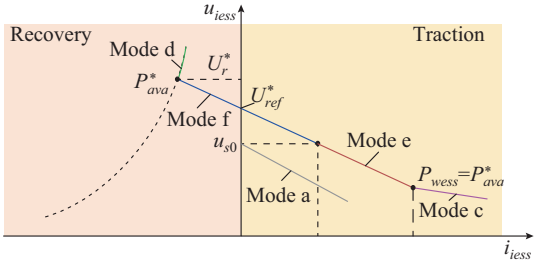

Fig. 7. External output characteristics of IESS under proposed method.

Specifically, in Fig. 7, when no usable capacity remains, the WESS is disconnected. At this point, if the voltage of traction grid is lower than the no-load voltage of substation, the IESS operates in mode a; otherwise, the IESS operates in mode b. When the WESS has usable capacity and the voltage of traction grid is lower than the no-load voltage of substation: if the operating point satisfies (13), the IESS operates in mode c; otherwise, the IESS operates in mode e. When the voltage of traction grid exceeds the no-load voltage of substation: if the power threshold P^*_{ava} is reached, the IESS operates in mode d; otherwise, the IESS operates in mode f. In Fig. 7, U^*_r is defined as the regulation voltage, which can be adjusted to modify the external output characteristics of the IESS. Finally, the output characteristics of modes e and f in (12) can be transformed into:

$$\begin{cases} u_{iess} = U^*_{ref} - \dfrac{(U^*_{ref})^2}{(P^*_{ava})^2}(1-\gamma)\gamma i_{iess} \\ \gamma = \dfrac{U^*_r - U^*_{iess}}{U^*_{iess}} \end{cases} \tag{14}$$

where γ is defined as the voltage regulation rate in modes e and f.

Based on the above analysis, the proposed method enables a unified classification for the operating modes of IESS into rigid and flexible modes. Rigid mode essentially corresponds to the inherent characteristics of substation, where the IESS operates in mode a or b, and its output characteristics are non-adjustable. Flexible modes correspond to modes c-f, where the output characteristics of IESS are adjustable. The control degrees of freedom include three parameters: U^*_{ref}, U^*_r (or r^*_{ref}), and P^*_{ava}. These allow for flexible regulation of the output characteristics of IESS based on the OPF framework.

B. Power Flow Model of DC TPS with IESS

The proposed method enables a unified representation of its output characteristics while decoupling the gird side from the energy storage side. Establishing a steady-state equivalent model of the DC TPS with IESS is fundamental for optimizing power flow within the OPF framework and achieving flexible traction power supply. As an example, Fig. 8 illustrates the equivalent circuit model of a DC TPS with two IESSs in a typical double-side power supply section.

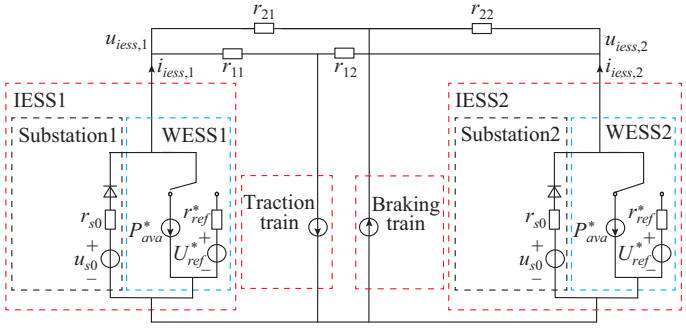

Fig. 8. Equivalent circuit model of DC TPS with two IESSs in typical double-side power supply section.

Based on the previous analysis, the rigid region of IESS corresponds to a conventional traction rectifier unit, while the flexible region can be represented as a switchable voltage source with internal resistance and constant power. Based on the steady-state analysis, the classic Newton-Raphson method can be used to solve the power flow of the DC TPS with IESSs. Similarly, the train can be modeled as a power source. Its power at different positions, derived from train traction calculation (TTC) or measured data, reflects the dynamic movement [28]. Therefore, the node location and power of train can be used as inputs for power flow calculations. The modified equation for the DC traction grid is shown in (15), which is used to solve the DC power flow under various operating conditions.

$$\begin{bmatrix} \Delta P_{dc,1} \\ \vdots \\ \Delta P_{dc,n} \end{bmatrix} = \begin{bmatrix} U_{dc,1}\dfrac{\partial \Delta P_{dc,1}}{\partial U_{dc,1}} & \cdots & U_{dc,n}\dfrac{\partial \Delta P_{dc,1}}{\partial U_{dc,n}} \\ \vdots & & \vdots \\ U_{dc,1}\dfrac{\partial \Delta P_{dc,n}}{\partial U_{dc,1}} & \cdots & U_{dc,n}\dfrac{\partial \Delta P_{dc,n}}{\partial U_{dc,n}} \end{bmatrix} \begin{bmatrix} \dfrac{\Delta U_{dc,1}}{U_{dc,1}} \\ \vdots \\ \dfrac{\Delta U_{dc,n}}{U_{dc,n}} \end{bmatrix} \tag{15}$$

where $U_{dc,i}$ is the voltage at node i of the DC traction grid; and $\Delta P_{dc,i}$ and $\Delta U_{dc,i}$ are the mismatch power and voltage at node i of the DC traction grid, respectively.

Under the proposed method, five distinct operating conditions must be considered, corresponding to the six operating modes of IESS discussed earlier.

1) When the IESS operates in mode a, the power mismatch of node i and the corresponding elements in the Jacobian matrix are expressed as:

$$\Delta P_{dc,i} = P_{iess,i} - P_{t,i} - U_{dc,i}\sum_{j=1,j\neq i}^{n} G_{dc,ij}\,(U_{dc,j} - U_{dc,i}) = \frac{U_{dc,i}(u_{s0} - U_{dc,i})}{r_{s0}} - P_{t,i} - U_{dc,i}\sum_{j=1,j\neq i}^{n} G_{dc,ij}\,(U_{dc,j} - U_{dc,i}) \tag{16}$$

$$\begin{cases} U_{dc,j}\dfrac{\partial \Delta P_{dc,i}}{\partial U_{dc,j}} = -U_{dc,j}G_{dc,ij}U_{dc,i} \\ U_{dc,i}\dfrac{\partial \Delta P_{dc,i}}{\partial U_{dc,i}} = \dfrac{U_{dc,i}(u_{s0} - 2U_{dc,i})}{r_{s0}} - P_{dc,i} + U_{dc,i}^2 G_{dc,ij} \end{cases} \tag{17}$$

where $P_{iess,i}$ and $P_{t,i}$ are the power of IESS and train at node i of the DC traction grid, respectively; and $G_{dc,ij}$ is the conductance between nodes i and j of DC traction grid.

2) When the IESS operates in mode b, the power mismatch of node i and the corresponding elements in the Jacobian matrix are expressed as:

$$\Delta P_{dc,i} = -P_{t,i} - U_{dc,i}\sum_{j=1,j\neq i}^{n} G_{dc,ij}\,(U_{dc,j} - U_{dc,i}) \tag{18}$$

$$\begin{cases} U_{dc,j}\dfrac{\partial \Delta P_{dc,i}}{\partial U_{dc,j}} = -U_{dc,j}G_{dc,ij}U_{dc,i} \\ U_{dc,i}\dfrac{\partial \Delta P_{dc,i}}{\partial U_{dc,i}} = -P_{dc,i} + U_{dc,i}^2 G_{dc,ij} \end{cases} \tag{19}$$

3) When the IESS operates in mode c, the power mismatch of node i is expressed as (20). The elements in the Jacobian matrix remain the same as (17).

$$\Delta P_{dc,i} = P_{iess,i} - P_{t,i} - U_{dc,i}\sum_{j=1,j\neq i}^{n} G_{dc,ij}\,(U_{dc,j} - U_{dc,i}) = \frac{U_{dc,i}(u_{s0} - U_{dc,i})}{r_{s0}} + P_{ava}^{*} - P_{t,i} - U_{dc,i}\sum_{j=1,j\neq i}^{n} G_{dc,ij}\,(U_{dc,j} - U_{dc,i}) \tag{20}$$

4) When the IESS operates in mode d, the power mismatch of node i is expressed as (21). The elements in the Jacobian matrix remain the same as (19).

$$\Delta P_{dc,i} = P_{iess,i} - P_{t,i} - U_{dc,i}\sum_{j=1,j\neq i}^{n} G_{dc,ij}\,(U_{dc,j} - U_{dc,i}) = P_{ava}^{*} - P_{t,i} - U_{dc,i}\sum_{j=1,j\neq i}^{n} G_{dc,ij}\,(U_{dc,j} - U_{dc,i}) \tag{21}$$

5) When the IESS operates in operating mode e or f, the power mismatch of node i and the corresponding elements in the Jacobian matrix are expressed as:

$$\Delta P_{dc,i} = P_{iess,i} - P_{t,i} - U_{dc,i}\sum_{j=1,j\neq i}^{n} G_{dc,ij}\,(U_{dc,j} - U_{dc,i}) = \frac{U_{dc,i}(U_{ref}^{*} - U_{dc,i})}{(U_{ref}^{*})^2(1-\gamma)\gamma}(P_{ava}^{*})^2 - P_{t,i} - U_{dc,i}\sum_{j=1,j\neq i}^{n} G_{dc,ij}\,(U_{dc,j} - U_{dc,i}) \tag{22}$$

$$\begin{cases} U_{dc,j}\dfrac{\partial \Delta P_{dc,i}}{\partial U_{dc,j}} = -U_{dc,j}G_{dc,ij}U_{dc,i} \\ U_{dc,i}\dfrac{\partial \Delta P_{dc,i}}{\partial U_{dc,i}} = \dfrac{U_{dc,i}(U_{ref}^{*} - 2U_{dc,i})}{(U_{ref}^{*})^2(1-\gamma)\gamma}(P_{ava}^{*})^2 - P_{dc,i} + U_{dc,i}^2 G_{dc,ij} \end{cases} \tag{23}$$

C. OPF Problem of DC TPS with IESS

For DC TPS, the energy consumption primarily comprises three components, as defined in (24). Notably, when RBE cannot be fully absorbed and causes the grid voltage to rise beyond a certain threshold, braking resistors are activated to dissipate the excess RBE [33]. In URT systems, a conventional method is ultimately converting RBE into heat. Due to space limitations, the operating characteristics of braking resistors are not further elaborated here.

$$E_{sys} = E_{sub} + E_{br,loss} + E_{l,loss} = \int P_{sub}\,\mathrm{d}t + \int P_{br,loss}\,\mathrm{d}t + \int P_{l,loss}\,\mathrm{d}t \tag{24}$$

where E_{sys} is the total energy consumption of DC TPS; and E_{sub}, $E_{br,loss}$, and $E_{l,loss}$ are the energy consumptions of substation, braking resistor, and line resistance, respectively, and P_{sub}, $P_{br,loss}$, and $P_{l,loss}$ are their corresponding power.

Therefore, in actual multi-station and multi-train scenarios, the OPF objectives for the DC TPS with IESS are expressed as:

$$\min f(x) = \min E_{sys} = \min\left(\sum_{m=1}^{M}\int_0^T P_{sub,m}\,dt + \sum_{n=1}^{N}\int_0^T P_{br,loss,n}\,\mathrm{d}t + \int_0^T P_{l,loss}\,\mathrm{d}t\right) \tag{25}$$

where M is the number of substations; N is the number of trains; and T is the operating period.

Under the integrated control, the vector of optimization variables $\boldsymbol{x}$ in the OPF framework is defined as (26). For

conventional substations, their operating modes alternate between modes a and b, corresponding to rigid conditions, and thus they have no associated optimization variables. The OPF constraints are specified in (27).

$$\boldsymbol{x}=[U^*_{ref,1}, U^*_{r,1}, P^*_{ava,1}, ..., U^*_{ref,M}, U^*_{r,M}, P^*_{ava,M}] \tag{26}$$

s.t.

$$\begin{cases} P_{iess,i}-P_{t,i}=U_{dc,i}\sum_{j=1,j\neq i}^{n} G_{dc,ij}(U_{dc,j}-U_{dc,i}) \\ SOC_{\min}\le SOC\le SOC_{\max} \\ U_{dc,\min}\le U_t\le U_{br,lim} \end{cases} \tag{27}$$

where $U^*_{ref,M}$, $U^*_{r,M}$, and $P^*_{ava,M}$ are the reference voltage, regulation voltage, and adjustable power limit of the IESS control loop at substation M, respectively; $SOC_{\min}$ and $SOC_{\max}$ are the minimum and maximum operating capacity of the designed energy storage, respectively; U_t is the voltage at the pantograph of train, which must meet the minimum voltage limitation $U_{dc,\min}$ for train operation; and $U_{br,lim}$ is the limit voltage of on-board braking resistors.

Regarding the optimization method, this paper does not address the relatively complex issue of online OPF. However, as discussed earlier, for energy storage components such as SC, which is the focus of this study, the available power is coupled with the remaining energy capacity. In other words, the power boundary dynamically changes with the variation in SOC. Therefore, the problem is not a static optimization under fixed constraints. Nevertheless, the offline optimization cannot track the real-time SOC, making it impossible to dynamically optimize and adjust P^*_{ava}. Therefore, in this study, the power threshold is temporarily set to the minimum available power across the entire operating range of the energy storage. Taking SC as an example, P^*_{ava} can be set as:

$$P^*_{ava}=\min P_{ava,\max}=I_{es,\max}u_{es,\min} \tag{28}$$

Using design parameters, (28) can be formulated based on (6) as:

$$\begin{cases} SOC_{\min}=u^2_{es,\min}/u^2_{sc,\max} \\ P^*_{ava}=\sqrt{SOC_{\min}}\,P_{es,\max} \end{cases} \tag{29}$$

These parameters can be determined during the design phase. It is important to note that the parameter settings constrain the power usage of energy storage but do not reduce its storage capacity, ensuring the total storable energy remains unaffected. The effects of these parameter settings will be discussed in detail in Section IV.

At this point, the OPF problem is transformed into a nonlinear optimization under fixed constraints, where the objective is defined by (25) and the optimization variables are limited to the two control parameters of energy storage substation: the reference voltage U^*_{ref} and regulation voltage U^*_r. A double-layer optimization structure is employed for solving the OPF problem studied in this paper, as shown in Fig. 9. The outer layer utilizes the classical heuristic algorithm and GA to conduct a large-scale global search for determining the initial values of optimization parameters. In the inner layer, traditional nonlinear optimization methods are used to further refine the results obtained from the outer-layer search. In this study, the sequential quadratic programming (SQP) is adopted as the inner-layer algorithm for OPF.

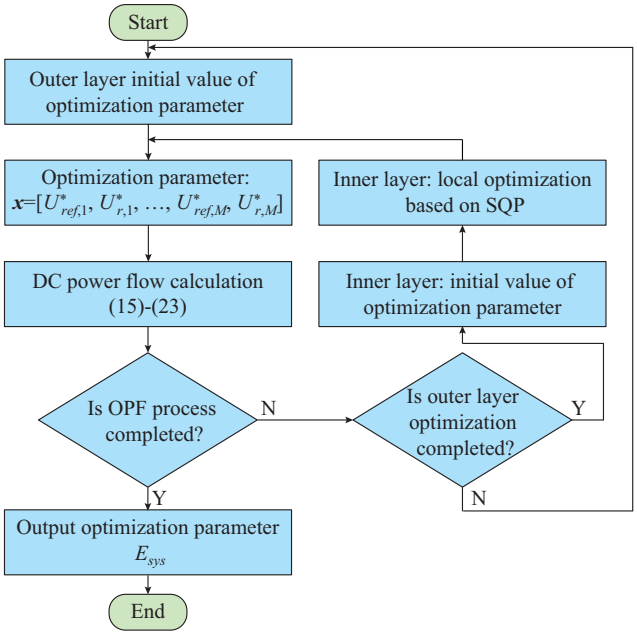

Fig. 9. Double-layer optimization structure for solving OPF problem.

IV. Case Studies

A. Case Conditions

This study takes a certain metro line in Beijing, China as the research subject and develops a TPS simulation model in multi-train operation scenarios, based on actual line conditions [34]. As shown in Fig. 10, the selected power supply section includes five IESSs (IESS1-IESS5). The differences in the no-load voltages of substations (Substations I-V) are also taken into account. Due to space limitations, the detailed parameters, configurations, and hardware environment of the TPS simulation can be found in Supplementary Material A.

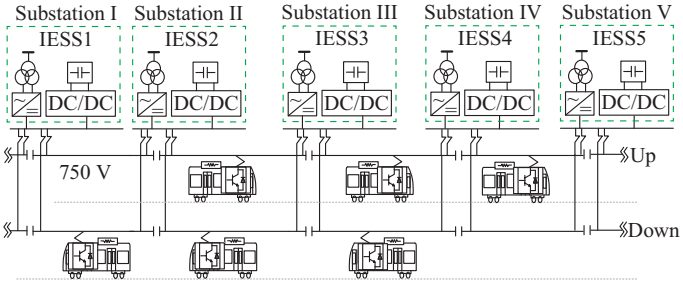

Fig. 10. Diagram of TPS configuration.

Extensive studies have been conducted on DC TPS calculation for URT systems [13], [35], [36]. Similarly, the URT TPS simulation platform has been well developed based on our previous works [4], [31]. Detailed descriptions of the simulation platform are omitted in this paper. To address the time-varying topology and parameter changes caused by

train movement, the virtual train modules are established within each section between two adjacent substations. Based on the displacement-time and power-time profiles of a single train in different power supply sections, the single-train operation curves are assigned to multiple virtual trains in various sections considering the train dispatch interval. During simulation, as the time step progresses, the power and displacement of train are updated through a table-lookup mechanism, while the line impedance dynamically varies with the position of train.

B. Optimization Results

In the scenario with a 7-min dispatch interval for the train, the optimized control parameters and energy consumption results are shown in Table I. To reduce the complexity of parameter optimization, all IESSs along the line share identical control variables and are optimized uniformly in the case study. The total execution time for the iterative optimization and simulation cycles is 3.6 hours, which is acceptable for a day-ahead offline optimization strategy. After optimization, the energy consumed by the braking resistors E_{br} is less than 0.5 kWh, indicating that the proposed method nearly achieves full utilization of RBE. At any given time, the total power of all trains within a power supply section is aggregated to approximate the load demand of the traction grid, taking into account energy exchange among trains.

TABLE I
OPTIMIZED CONTROL PARAMETERS AND ENERGY CONSUMPTION RESULTS

Control parameter		Energy consumption		
U_{ref}^{*} (V)	U_{r}^{*} (V)	E_{sub} (kWh)	E_{br} (kWh)	E_{loss} (kWh)
861	846	103.57	0.49	7.84

A comparison between the TPS load demand and the aggregated power output of all IESSs is illustrated in Fig. 11. As shown in Fig. 11, the proposed method enables the TPS power flow to fully accommodate the TPS load demand. When RBE remains in the system after the train energy interactions ($P_{load}<0$), the IESSs effectively recover the surplus energy. When the traction energy is required ($P_{load}\geq 0$), the IESSs supplement the demand by discharging energy. Figure 12 shows the voltages of traction grid measured at various substations. It can be observed that the overall voltage level remains low, with no significant overvoltage events exceeding the 900 V threshold for braking resistor activation. This is consistent with the results shown in Table I, where nearly no energy is dissipated through the braking resistors. During the majority of the time, the grid voltage demonstrates good regulation performance, with a minimum voltage of 797 V. Compared with the minimum no-load voltage of the substations, the voltage drop is approximately 3%.

C. Performance Comparison of Different EMSs

Under the same energy storage configuration, Table II presents the energy-saving performance of the TPS under different control strategies. The energy-saving rate e% is calculated using:

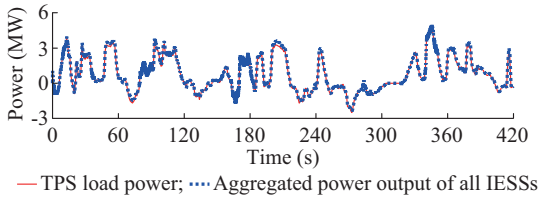

Fig. 11. Comparison between TPS load demand and aggregated power output of all IESSs.

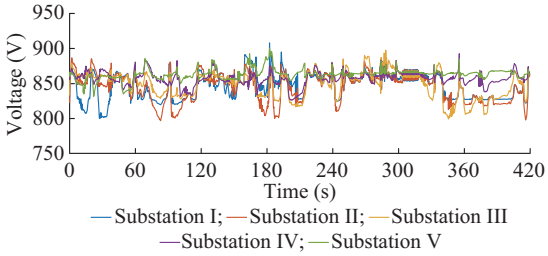

Fig. 12. Voltages of traction grid measured at various substations.

TABLE II
ENERGY-SAVING PERFORMANCE OF TPS UNDER DIFFERENT CONTROL STRATEGIES

Strategy	E_{br} (kWh)	E_{sys} (kWh)	e%
Without WESS	30.45	160.77	
Strategy 1	4.61	126.93	21.05%
Strategy 2	1.03	116.13	27.77%
Strategy 3	0.49	111.90	30.40%

$$e\% = \frac{E_{sys,nowess} - E_{sys}}{E_{sys,nowess}} \times 100\% \tag{30}$$

where $E_{sys,nowess}$ is the system energy consumption without WESS.

The following three control strategies (strategies 1-3) are defined.

1) Strategy 1: a threshold-based control strategy using the no-load voltage of substation as reference for charging/discharging decisions, which is also the most widely applied strategy in practice [16], [37].

2) Strategy 2: a distributed optimization strategy that uses the system energy consumption as the objective in (25), applying a GA to optimize the WESS threshold values to reference U_{ref} at each substation [24]. The optimized voltage thresholds are 837 V, 842 V, 852 V, 857 V, and 858 V, respectively. Strategies 1 and 2 both adopt the traditional control approach shown in Fig. 2, which only considers the WESS in isolation.

3) Strategy 3: the proposed method. Table II shows that the proposed method (strategy 3) achieves the best energy-saving performance. Compared with strategies 1 and 2, the proposed method improves the energy-saving rate by 9% and 3%, respectively, relative to the threshold-setting approaches based on the no-load voltage and distributed GA optimization. Figure 13 shows the energy consumption of substation under different control strategies. Compared with strategies 1 and 2, the proposed method reduces the energy

consumption of substation by 10% and 4%, respectively. In addition, regarding the energy consumption by braking resistors E_{br}, the proposed method results in reductions of 89% and 53%, respectively.

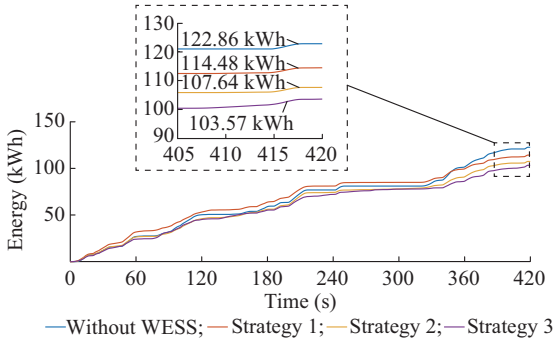

Fig. 13. Energy consumption of substation under different control strategies.

Figure 14 illustrates the energy consumption per minute of the braking resistors under different control strategies.

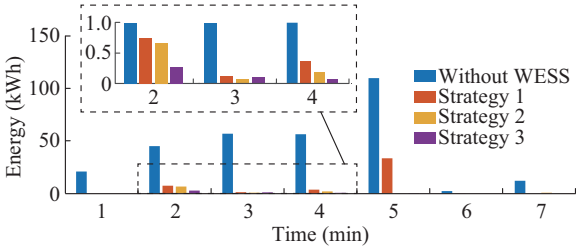

Fig. 14. Energy consumption per minute of braking resistor under different control strategies.

Since strategies 1 and 2 do not impose a power threshold on the WESS, the systems are theoretically allowed to operate at their maximum power capacities. Figure 15 presents the actual power contribution of the WESS at each substation under different control strategies. Under strategies 1 and 2, the maximum absolute power outputs reach 1.77 MW and 1.24 MW, respectively. In contrast, under the proposed method, i.e., strategy 3, all WESSs operate below 1 MW due to the imposed power limit. Although the energy storage capacity remains unchanged, strategy 3 effectively reduces the required capacity of power converter. Moreover, this strategy achieves the best energy-saving performance while lowering the power demand, further demonstrating the uniqueness and superiority of the proposed method.

Furthermore, the simulation results indicate a coupling relationship between the configuration of energy storage capacity and energy management. Adopting a rational and efficient control method can not only enhance the energy-saving performance but also optimize the configuration of energy storage capacity, thereby further improving the system economic efficiency.

Figure 16 illustrates the SOC of WESS under different control strategies. It can be observed that the proposed method has the lowest capacity demand. Throughout the operating cycle, the actual utilized SOC of substations I and II is the minimal. This also suggests that under the proposed method, the configuration of current energy storage capacity still has redundancies. The optimization of capacity configuration in joint control strategies is also an important research topic.

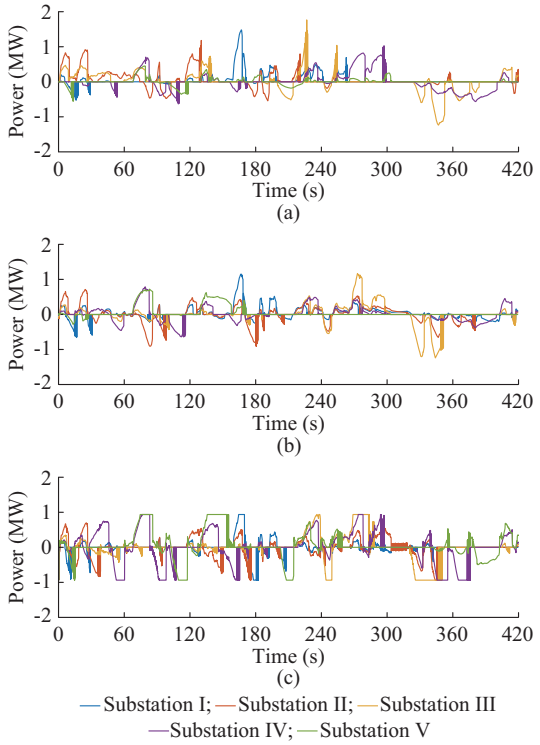

Fig. 15. Actual power contribution of WESS at each substation under different control strategies. (a) Strategy 1. (b) Strategy 2. (c) Strategy 3.

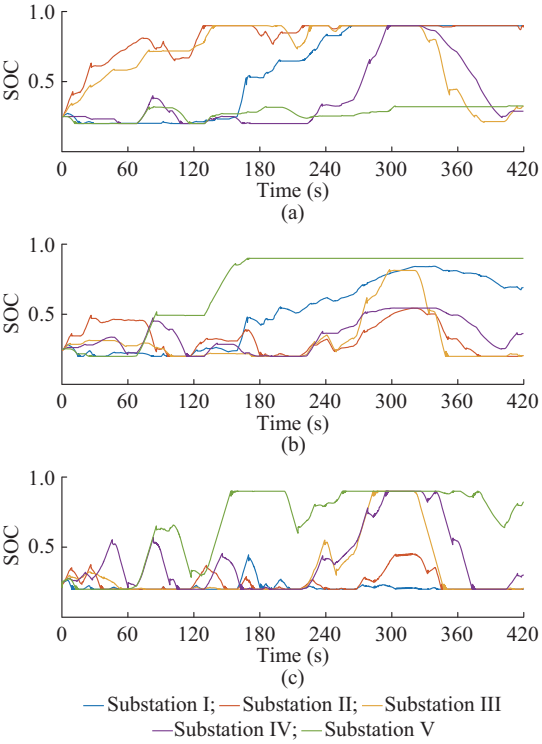

Fig. 16. SOC of WESS under different control strategies. (a) Strategy 1. (b) Strategy 2. (c) Strategy 3.

D. Robustness Verification of Proposed Method

To verify the robustness of the proposed method, its control performance is evaluated under different operating conditions. Figure 17 presents the actual train dispatch intervals on weekdays and weekends, where in non-optimized scenarios for train operation, no secondary optimization of control parameters is performed.

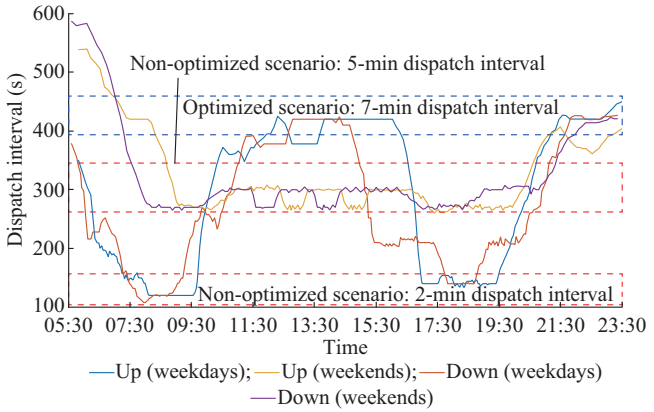

Fig. 17. Actual train dispatch intervals on weekdays and weekends.

Figure 18 shows the energy per minute and total energy consumption under different control strategies at various dispatch intervals. The results indicate that in two non-optimized scenarios, the proposed method still maintains favorable control characteristics and consistently achieves the best energy-saving performance among all strategies. Compared with strategies 1 and 2, the system energy consumption at the 5-min dispatch interval decreases from 136.07 kWh and 129.40 kWh to 127.58 kWh with the proposed method, achieving reductions of 6.2% and 1.4%, respectively. At shorter dispatch intervals, the energy interaction between the traction and braking trains is sufficient, leading to better intrinsic energy-saving performance of system. At the 2-min dispatch interval, the proposed method further reduces the system energy consumption from 107.17 kWh and 106.75 kWh to 104.03 kWh, achieving reductions of 2.9% and 2.5%, respectively.

These results demonstrate that even within a general offline OPF framework, the proposed method maintains effective control performance under varying operating conditions. This is because, even with fixed control parameters, the integrated control allows the output behavior of IESS to be dynamically adjusted in real time based on voltage of traction grid and current feedback of IESS, thereby enabling a certain degree of adaptive control. Furthermore, to handle real-world operating uncertainties, a control parameter library can be constructed offline based on representative train operation schedules. During the daily operation, the optimal control parameters of IESS can be adaptively selected according to the current status. Therefore, in view of the foregoing analysis on optimization complexity, the proposed method is particularly well suited as a day-ahead optimization strategy in engineering practice. Alternatively, the adaptive parameter optimization can also be achieved under the real-time OPF framework, further improving the energy-saving performance under different operating conditions. In summary, the proposed method demonstrates strong robustness, deploy-ability, and scalability, making it suitable for building URT FTPS.

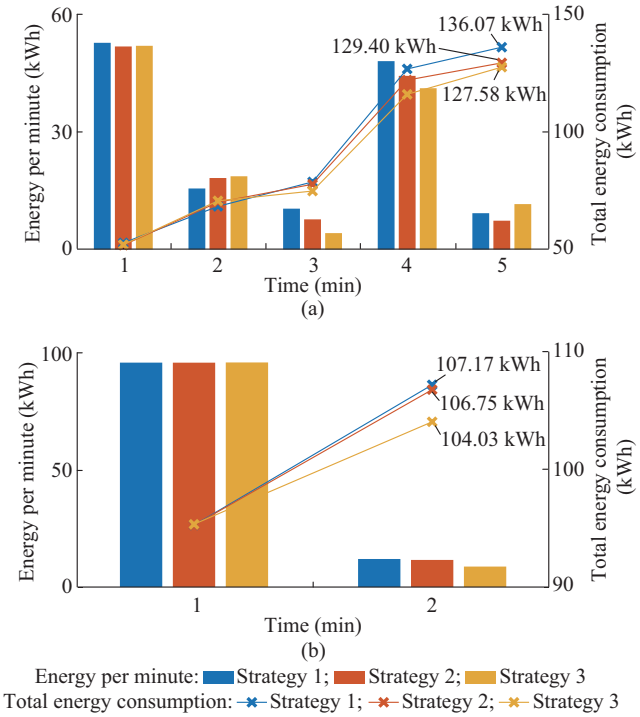

Fig. 18. Energy per minute and total energy consumption under different control strategies in various dispatch interval. (a) 5-min dispatch interval. (b) 2-min dispatch interval.

V. Conclusion

This work takes the WESS and substation into a unified IESS from a novel perspective, and proposes an integrated control method of TPS with WESS based on power flow optimization method. Based on the engineering conditions of a metro line, a case study of the proposed method is carried out. The proposed method greatly enhances the potential of applying WESS to improve energy-saving performance in URT. The important conclusions are summarized as follows.

1) The IESS control method is proposed for the first time. The steady-state equivalent model of IESS-based TPS is established. Moreover, within the general OPF framework, the optimization of power flow and flexible traction power supply in IESS-based TPS has been successfully achieved.

2) The results of case study based on engineering data show that compared with the most widely used method, the RBE loss can be reduced by 89% under long dispatch interval condition. Almost zero waste is achieved. Compared with the distributed optimization method, the RBE loss is still reduced by 53%.

3) The proposed method allows WESS to operate at lower power levels, which reduces the capacity design of energy storage converters, thereby improving the economic-efficiency.

Finally, regarding the construction of FTPS based on IESSs, several research areas remain to be explored.

1) Online OPF method for IESS-based TPS needs to be

developed. Control parameters should be optimized online according to the system state at different moments, including real-time tracking of energy storage capacity status and adjusting power thresholds. Investigating energy-saving potential by real-time OPF is crucial.

2) Case study results indicate that the proposed method offers significant advantages in reducing energy storage capacity and power demand. Therefore, from the perspective of improving economic efficiency, exploring joint optimization strategies for control and capacity configuration holds substantial value.

REFERENCES

[1] China Urban Rail Transit Association. (2025, May). Urban rail transits the statistics and analysis report 2024. [Online]. Available: https://www.camet.org.cn/xytj/tjxx/660844283682885.shtml

[2] M. Chen, X. Feng, Y. Guo *et al*., "Optimal cooperative eco-driving of multitrain with TLET comprehensive system," *IEEE Transactions on Transportation Electrification*, vol. 10, no. 1, pp. 2095-2111, Jun. 2023.

[3] Z. Feng, W. Chen, Y. Liu *et al*., "Long-term equilibrium relationship analysis and energy-saving measures of metro energy consumption and its influencing factors based on cointegration theory and an ARDL model," *Energy*, vol. 263, p. 125965, Jan. 2023.

[4] J. Mi, Z. Yang, Z. Zhong *et al*., "Research on current and power tracing in urban rail transit," *Proceedings of the CSEE*, vol. 44, no. 6, pp. 2270-2278, Mar. 2024.

[5] J. Zhang, Z. Tian, W. Liu *et al*., "Regenerative braking energy utilization analysis in AC/DC railway power supply system with energy feedback systems," *IEEE Transactions on Transportation Electrification*, vol. 10, no. 1, pp. 239-251, Mar. 2024.

[6] Z. Li, X. Li, Y. Wei *et al*., "Fast quasi-optimal power flow of flexible DC traction power systems," *IEEE Transactions on Power Systems*, vol. 39, no. 1, pp. 1555-1567, Jan. 2024.

[7] F. Hao, G. Zhang, J. Chen *et al*., "Optimal voltage regulation and power sharing in traction power systems with reversible converters," *IEEE Transactions on Power Systems*, vol. 35, no. 4, pp. 2726-2735, Jul. 2020.

[8] J. Chen, H. Hu, M. Wang *et al*., "Power flow control-based regenerative braking energy utilization in AC electrified railways: review and future trends," *IEEE Transactions on Intelligent Transportation Systems*, vol. 25, no. 7, pp. 6345-6365, Jan. 2024.

[9] Y. Ying, Q. Liu, M. Wu *et al*., "Online energy management strategy of the flexible smart traction power supply system," *IEEE Transactions on Transportation Electrification*, vol. 9, no. 1, pp. 981-994, Jul. 2022.

[10] H. Hu, X. Meng, X. Yang *et al*., "A hierarchical control strategy for the novel 24 kV flexible direct current railway traction power system," *Proceedings of the CSEE*, vol. 41, no. 10, pp. 3373-3382, May 2021.

[11] Y. Ying, Z. Tian, M. Wu *et al*., "A real-time energy management strategy of flexible smart traction power supply system based on deep *Q*-learning," *IEEE Transactions on Intelligent Transportation Systems*, vol. 25, no. 8, pp. 8938-8948, Jun. 2024.

[12] M. Domínguez, A. Fernández-Cardador, A. Fernández-Rodríguez *et al*., "Review on the use of energy storage systems in railway applications," *Renewable and Sustainable Energy Reviews*, vol. 207, p. 114904, Jan. 2025.

[13] M. Khodaparastan, O. Dutta, M. Saleh *et al*., "Modeling and simulation of DC electric rail transit systems with wayside energy storage," *IEEE Transactions on Vehicular Technology*, vol. 68, no. 3, pp. 2218-2228, Mar. 2019.

[14] D. Ramsey, T. Letrouve, A. Bouscayrol *et al*., "Comparison of energy recovery solutions on a suburban DC railway system," *IEEE Transactions on Transportation Electrification*, vol. 7, no. 3, pp. 1849-1857, Sept. 2021.

[15] J. Luo, X. Wei, S. Gao *et al*., "Summary and outlook of capacity configuration and energy management technology of high-speed railway energy storage system," *Proceedings of the CSEE*, vol. 42, no. 19, pp. 7028-7050, Oct. 2022.

[16] F. Ciccarelli, D. Iannuzzi, K. Kondo *et al*., "Line-voltage control based on wayside energy storage systems for tramway networks," *IEEE Transactions on Power Electronics*, vol. 31, no. 1, pp. 884-899, Jan. 2016.

[17] F. Zhu, Z. Yang, F. Lin *et al*., "Dynamic threshold adjustment strategy of supercapacitor energy storage system based on no-load voltage identification in urban rail transit," in *Proceedings of 2019 IEEE Transportation Electrification Conference and Expo Asia-Pacific*, Seogwipo, Korea, May 2019, pp. 1-6.

[18] F. Meishner and D. U. Sauer, "Wayside energy recovery systems in DC urban railway grids," *eTransportation*, vol. 1, p. 100001, Aug. 2019.

[19] Y. Zhao, Z. Zhong, F. Lin *et al*., "Multi time scale management and coordination strategy for stationary super capacitor energy storage in urban rail transit power supply system," *Electric Power Systems Research*, vol. 228, p. 110046, Mar. 2024.

[20] K. Sun, Z. Yang, F. Lin *et al*., "Energy management strategy of multiple energy storage systems in urban railway based on train operating status.," in *Proceedings of 2023 IEEE 3rd International Conference on Industrial Electronics for Sustainable Energy Systems*, Shanghai, China, Jul. 2023, pp. 1-6.

[21] S. Yang, Y. Chen, Z. Dong *et al*., "A collaborative operation mode of energy storage system and train operation system in power supply network," *Energy*, vol. 276, p. 127617, Aug. 2023.

[22] W. Jin, Y. Gao, H. Zhang *et al*., "Real-time power tracking control for supercapacitor-based regenerative braking system using interacting multiple model filter," *IEEE Transactions on Vehicular Technology*, vol. 72, no. 9, pp. 11437-11445, Apr. 2023.

[23] H. Dong, Z. Tian, J. W. Spencer *et al*., "Coordinated control strategy of railway multisource traction system with energy storage and renewable energy," *IEEE Transactions on Intelligent Transportation Systems*, vol. 24, no. 12, pp. 15702-15713, May 2023.

[24] H. J. Kaleybar, M. Davoodi, M. Brenna *et al*., "Applications of genetic algorithm and its variants in rail vehicle systems: a bibliometric analysis and comprehensive review," *IEEE Access*, vol. 11, pp. 68972-68993, Jul. 2023.

[25] F. Zhu, Z. Yang, F. Lin *et al*., "Decentralized cooperative control of multiple energy storage systems in urban railway based on multiagent deep reinforcement learning," *IEEE Transactions on Power Electronics*, vol. 35, no. 9, pp. 9368-9379, Feb. 2020.

[26] J. Luo, Y. Wang, S. Gao *et al*., "Multiagent-game-based reinforcement learning energy management strategy for flexible traction power supply system with energy storage system," *IEEE Transactions on Transportation Electrification*, vol. 11, no. 3, pp. 8474-8488, Jun. 2025.

[27] X. Wang, Y. Luo, B. Qin *et al*., "Power allocation strategy for urban rail HESS based on deep reinforcement learning sequential decision optimization," *IEEE Transactions on Transportation Electrification*, vol. 9, no. 2, pp. 2693-2710, Dec. 2022.

[28] Z. Yang, F. Zhu, and F. Lin, "Deep-reinforcement-learning-based energy management strategy for supercapacitor energy storage systems in urban rail transit," *IEEE Transactions on Intelligent Transportation Systems*, vol. 22, no. 2, pp. 1150-1160, Jan. 2020.

[29] P. Pozzobon, "Transient and steady-state short-circuit currents in rectifiers for DC traction supply," *IEEE Transactions on Vehicular Technology*, vol. 47, no. 4, pp. 1390-1404, Nov. 1998.

[30] T. Ratniyomchai, S. Hillmansen, and P. Tricoli, "Recent developments and applications of energy storage devices in electrified railways," *IET Electrical Systems in Transportation*, vol. 4, no. 1, pp. 9-20, Mar. 2014.

[31] Y. Liu, Z. Yang, X. Wu *et al*., "An adaptive energy management strategy of stationary hybrid energy storage system," *IEEE Transactions on Transportation Electrification*, vol. 8, no. 2, pp. 2261-2272, Jun. 2022.

[32] X. Lu, J. M. Guerrero, K. Sun *et al*., "An improved droop control method for DC microgrids based on low bandwidth communication with DC bus voltage restoration and enhanced current sharing accuracy," *IEEE Transactions on Power Electronics*, vol. 29, no. 4, pp. 1800-1812, Jun. 2013.

[33] X. Shen, H. Wei, and T. T. Lie, "Management and utilization of urban rail transit regenerative braking energy based on the bypass DC loop," *IEEE Transactions on Transportation Electrification*, vol. 7, no. 3, pp. 1699-1711, Sept. 2021.

[34] F. Zhu, Z. Yang, Z. Zhao *et al*., "Two-stage synthetic optimization of supercapacitor-based energy storage systems, traction power parameters and train operation in urban rail transit," *IEEE Transactions on Vehicular Technology*, vol. 70, no. 9, pp. 8590-8605, Sept. 2021.

[35] D. Yu, K. L. Lo, X. Wang *et al*., "MRTS traction power supply system simulation using MATLAB/Simulink," in *Proceedings of IEEE 55th Vehicular Technology Conference,* Birmingham, USA, Aug. 2002, pp. 308-312.

[36] F. Ciccarelli, D. Iannuzzi, and D. Lauria, "Supercapacitors-based ener-

gy storage for urban mass transit systems," in *Proceedings of the 2011 14th European Conference on Power Electronics and Applications*, Birmingham, UK, Aug. 2011, pp. 1-10.
[37] V. A. Kleftakis and N. D. Hatziargyriou, "Optimal control of reversible substations and wayside storage devices for voltage stabilization and energy savings in metro railway networks," *IEEE Transactions on Transportation Electrification*, vol. 5, no. 2, pp. 515-523, Apr. 2019.

Yan Li received the B.S. and M.S. degrees in electrical engineering from Beijing Jiaotong University, Beijing, China, in 2018 and 2020, respectively, where he is currently working toward the Ph.D. degree with the School of Electrical Engineering. His research interests include development and application of machine learning (ML) in energy storage modeling and optimization of energy management in urban rail transit.

Fei Lin received the B.S. degree from Xi'an Jiaotong University, Xi'an, China, in 1997, the M.S. degree from Shandong University, Jinan, China, in 2000, and the Ph.D. degree from Tsinghua University, Beijing, China, in 2004, all in electrical engineering. He is currently a Professor with the School of Electrical Engineering, Beijing Jiaotong University, Beijing, China. His research interests include traction converter, energy management for railway system, and digital control.

Zhongping Yang received the B.Eng. degree from the Tokyo University of Mercantile Marine, Tokyo, Japan, in 1997, and the M.Eng. and Ph.D. degrees from The University of Tokyo, Tokyo, Japan, in 1999 and 2002, respectively, all in electrical engineering. He is currently a Professor with the School of Electrical Engineering, Beijing Jiaotong University, Beijing, China. His research interests include high-speed rail technology, regenerative braking energy utilization technology, and wireless power transmission.

Xiaochun Fang received the B.S. and Ph.D. degrees in engineering from Beijing Jiaotong University, Beijing, China, in 2010 and 2016, respectively. He is currently an Associate Professor with the School of Electrical Engineering, Beijing Jiaotong University. His current research interests include motor drive, insulated gate bipolar transistor (IGBT) fault mechanism, and failure prediction.

Hu Sun received the B.S. and M.S. degrees from North China Electric Power University, Baoding, China. He is currently a Senior Engineer with the Institute of Power Electronics, School of Electrical Engineering, Beijing Jiaotong University, Beijing, China. His current research interests include technical research on energy mutual feed test control system for electric traction AC drive and converter detection test system.

Zhihong Zhong received the B.S. and Ph.D. degrees in electrical engineering from Beijing Jiaotong University, Beijing, China, in 2015 and 2020, respectively. His research interests include modeling and optimization of energy storage system and motor drive.